AGU PUBLICATIONS

JGR

Journal of Geophysical Research: Atmospheres

RESEARCH ARTICLE
10.1002/2014JD022966

Key Points:
- Aerosol optical properties and CCN activity at high-altitude Himalayas
- CCN concentration is high when aerosol absorption is also high
- Seasonality in CCN activity over Himalayas

Correspondence to:
S. S. Babu,
s_sureshbabu@vssc.gov.in

Citation:
Gogoi, M. M., S. S. Babu, V. Jayachandran, K. K. Moorthy, S. K. Satheesh, M. Naja, and V. R. Kotamarthi (2015), Optical properties and CCN activity of aerosols in a high-altitude Himalayan environment: Results from RAWEX-GVAX, *J. Geophys. Res. Atmos.*, *120*, 2453–2469, doi:10.1002/2014JD022966.

Received 10 DEC 2014
Accepted 19 FEB 2015
Accepted article online 24 FEB 2015
Published online 28 MAR 2015

Optical properties and CCN activity of aerosols in a high-altitude Himalayan environment: Results from RAWEX-GVAX

Mukunda M. Gogoi[1], S. Suresh Babu[1], V. Jayachandran[1], K. Krishna Moorthy[2], S. K. Satheesh[3], Manish Naja[4], and V. R. Kotamarthi[5]

[1]Space Physics Laboratory, Vikram Sarabhai Space Centre, Thiruvananthapuram, India, [2]Indian Space Research Organization Head Quarters, Bangalore, India, [3]Centre for Atmospheric and Oceanic Sciences, Indian Institute of Science, Bangalore, India, [4]Aryabhatta Research Institute of Observational Sciences, Nainital, India, [5]Environmental Research Division, Argonne National Laboratory, Argonne, Illinois, USA

Abstract The seasonality and mutual dependence of aerosol optical properties and cloud condensation nuclei (CCN) activity under varying meteorological conditions at the high-altitude Nainital site (~2 km) in the Indo-Gangetic Plains were examined using nearly year-round measurements (June 2011 to March 2012) at the Atmospheric Radiation Measurement mobile facility as part of the Regional Aerosol Warming Experiment–Ganges Valley Aerosol Experiment of the Indian Space Research Organization and the U.S. Department of Energy. The results from collocated measurements provided enhanced aerosol scattering and absorption coefficients, CCN concentrations, and total condensation nuclei concentrations during the dry autumn and winter months. The CCN concentration (at a supersaturation of 0.46) was higher during the periods of high aerosol absorption (single scattering albedo (SSA) < 0.80) than during the periods of high aerosol scattering (SSA > 0.85), indicating that the aerosol composition seasonally changes and influences the CCN activity. The monthly mean CCN activation ratio (at a supersaturation of 0.46) was highest (>0.7) in late autumn (November); this finding is attributed to the contribution of biomass-burning aerosols to CCN formation at high supersaturation conditions.

1. Introduction

Aerosol characterization over South and Southeast Asia has attracted considerable attention in recent years because of (a) the rapid development and increasing population in these regions, (b) the complex combination of anthropogenic activities and distinct natural sources that contribute to regional aerosol characteristics, and (c) the implications for the regional and global climate [*Moorthy et al.*, 2013; *Lawrence and Lelieveld*, 2010]. In particular, the Ganges Valley region, which is commonly known as the Indo-Gangetic Plain (IGP), is an aerosol hot spot in South Asia. In addition to the extensive anthropogenic activities in the region, several other factors (meteorological and orographical) are conducive to the advection of aerosols from the west and to their confinement over the central and eastern parts of the IGP. These factors include prevailing anticyclonic winds, dry conditions, a gradual elevation drop, and topographical narrowing from west to east over the IGP, with the Himalayas to the north and the highlands of Bihar to the south. The low temperatures (as low as 0°C overnight in many parts of the IGP in winter) and the low wind speed ($<2\ m\ s^{-1}$) inhibit vertical (convective) and horizontal mixing of aerosols produced at the surface due to a shallow boundary layer and weak thermal convection. Therefore, a high aerosol load persists over this region in winter. The increasing aerosol load could lead to a large regional radiative imbalance in the Earth-atmosphere system through increased backscattering from anthropogenic aerosols, cloud burn off due to localized heating by black carbon (BC), and changes in cloud droplet size and abundance due to increased aerosol concentrations. The frequent winter fog is another cause for concern over the IGP.

The combined effects of all of these factors reportedly have a strong influence on the Asian monsoon circulations over the region [*Lawrence and Lelieveld*, 2010; *Gautam et al.*, 2009]. The consequences of the dynamic feedback of absorbing aerosols at high altitudes during hot summer monsoon seasons have already become a popular topic of the scientific community [e.g., *Marinoni et al.*, 2010]. During the nonmonsoon months, the transport of dust aerosols from arid locations to the west of the IGP enhances the aerosol loading in the atmosphere and leads to aerosol accumulation under dry conditions. To address these

issues, regular ground-based observations and periodic campaigns have supplemented satellite-based measurements for more than a decade [*Nair et al*., 2007; *Gautam et al*., 2011; *Srivastava et al*., 2012].

Interestingly, recent observations indicate warming in the upper atmosphere (atmospheric layers > 2 km) by aerosol absorption and northward directed height and amplitude gradients [*Satheesh et al*., 2008; *Babu et al*., 2011] over the Indian region; consequently, the pressure gradient between the land and the ocean may intensify and strengthen the Indian monsoon. Aerosols transported from the IGP reportedly have a strong influence on cloud formation and monsoon activity over the Indian Ocean. Enhanced cloud droplet concentrations reduce the atmospheric solar heating and convective mixing over the oceanic regions [*Ramanathan et al*., 2005, 2007]. Satellite mapping of the aerosol loading over the IGP has prevalently shown very large aerosol optical depths [*Massie et al*., 2004; *Girolamo et al*., 2004; *Prasad et al*., 2004; *Gautam et al*., 2009]. In fact, the analysis of more than two decades of data from the National Aeronautics and Space Administration Total Ozone Mapping Spectrometer has revealed a large, sustained increase in the aerosol loading over the IGP [*Massie et al*., 2004; *Habib et al*., 2006; *Sarkar et al*., 2006; *Bollasina et al*., 2008]. Based on Sun/sky radiometer observations during the premonsoon season, *Srivastava et al*. [2011] have reported that atmospheric absorption over the central IGP region is mainly due to the dominance of coarse-mode dust particles. During the same season, enhanced convective activity typically leads to atmospheric heating because of the lifting of dust and BC to higher altitudes, particularly in northern India [*Lau et al*., 2006]. Although a number of studies over the Indian region have focused on the direct effect of aerosols, the indirect effects of aerosols are not as well known.

In terms of the indirect effects of aerosols, one of the main challenges is to reduce the large uncertainties involved in quantitatively connecting the chemical compositions of aerosol particles to their hygroscopic growth and the consequences of their optical properties. Although the activation of aerosol particles for inducing cloud formation remains a topic of intense investigation [*Liu and Li*, 2014], understanding changes in the microphysical properties of clouds, cloud life spans, and the precipitation regimes influenced by atmospheric aerosols is important in quantifying the indirect effects of aerosols. The cloud condensation nuclei (CCN) activity of aerosols depends on both the aerosol size distribution and the supersaturation (SS). Quantification of these attributes for different aerosol types is important for understanding the indirect effects of aerosols on climate forcing. According to Köhler's theory, the saturation vapor pressure decreases as the size of a soluble particle increases (because of variations in the curved surface) and as the mass of a solute increases [*Lee et al*., 2010]. Thus, the aerosol size distribution, solubility, and hygroscopicity play major roles in complex aerosol-cloud interactions [*Lee et al*., 2010; *McFiggans et al*., 2006]. However, measurements of CCN concentrations are not globally abundant, particularly over India.

Earlier studies have revealed that the activation efficiency (fraction of total condensation nuclei (CN) activated as CCN) varies by aerosol type [*Burkart et al*., 2011]. For example, sulfate aerosols are considered the most effective CCN, with organic aerosols also significantly contributing to the global CCN budget [*Acker et al*., 2002; *Sun and Ariya*, 2006]. As reported in laboratory studies, cloud activation of particles containing BC is due to the condensation of hygroscopic compounds [*Lammel and Novakov*, 1995; *Petzold et al*., 2005]. However, ambient conditions are far more complex because various types of inorganic and organic compounds are mixed with BC (both externally and internally). Similarly, hygroscopic sulfate and nitrate coatings on coarse dust particles can enhance the CCN activation of dust [*Li et al*., 2011]. Although decades of research have substantially improved our knowledge of aerosol-cloud-precipitation interactions [*Stevens and Feingold*, 2009], uncertainties still persist. More observational data in specific environments are required to provide insight into cloud droplet formation, provide information for global climate models, and produce accurate predictions. Based on the limited studies over South and Southeast Asia, *Vinoj and Satheesh* [2004] have reported that the indirect radiative forcing of sea salt aerosols (ranging from $-4\,\mathrm{W\,m^{-2}}$ to $-18\,\mathrm{W\,m^{-2}}$) over the Arabian Sea is many times greater than their direct radiative forcing. Similarly, *Ramanathan et al*. [2001] have reported that the Indo-Asian haze produced a negative forcing of $-5 \pm 2\,\mathrm{W\,m^{-2}}$ at the top of the atmosphere because of the indirect effect of the elevated absorbing aerosol layer. Recent observational studies [*Pandithurai et al*., 2012] have also indicated a 15% decrease in the cloud droplet effective radius, which may increase a cloud's lifespan due to a 30% increase in the aerosol accumulation mode.

The above context suggests that extensive characterization of aerosols and CCN activity over the IGP are important. Collocated measurements of several aerosol parameters were obtained over the central

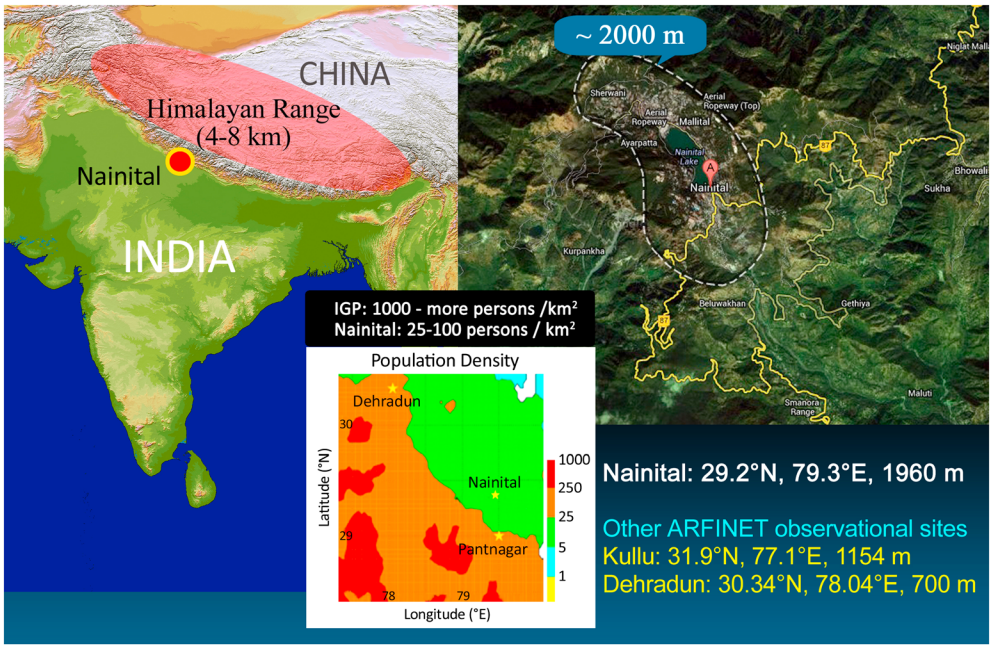

Figure 1. Geographic location of Nainital in the northern part of the Indian subcontinent.

Himalayan location of Nainital (29.2°N, 79.3°E, ~2 km above mean sea level (asl)) from June 2011 to March 2012. The measurements were part of the collaborative Regional Aerosol Warming Experiment (RAWEX) and the Ganges Valley Aerosol Experiment (GVAX). During these experiments, the AMF (Atmospheric Radiation Measurement (ARM) Program Mobile Facility of the U.S. Department of Energy) was deployed at Nainital for extensive measurements. Nainital was chosen as the optimal experimental site for studying the regional distribution of complex aerosol sources, transport, and direct and indirect radiative forcing mechanisms [*Kotamarthi and Satheesh*, 2011]. Several instruments were deployed at Nainital to measure the physical, optical, and chemical properties of aerosols for both near-surface and columnar characterization. The present study addresses the optical properties of aerosols and their association with CCN activity in different seasons. The ratio of the number of particles that act as CCN at a particular SS to the total number of condensation nuclei (CN) is defined here as the CCN activity. We report the aerosol CCN activity at a high-altitude location in the Himalayan foothills near an anthropogenic aerosol hot spot using nearly year-round data.

2. Site Description: Topography and Climate

Nainital is located in the central Himalayas (Figure 1) at an altitude of ~ 2 km asl. The aerosol measurements were performed at the Aryabhatta Research Institute for Observational Sciences observatory (http://www.aries.res.in/) at Manora Peak. At this elevation, the growth of the planetary boundary layer in the late afternoon plays a major role in transporting aerosols from the valleys to the site; as a result, significant perturbations in aerosol properties occur over the peak [*Sagar et al*., 2004; *Hegde et al*., 2007; *Dumka et al*., 2008, 2010]. Nainital is a well-known station, with thriving tourist activity during March–May. The general meteorological conditions at Nainital are monsoonal (heavy rainfall) from June to August, when the surface temperatures exhibit large diurnal fluctuations (rarely rising above 27°C). The temperatures are near zero from December to February (winter).

During the RAWEX-GVAX experiment period (June 2011 to March 2012), the monthly mean temperature (Figure 2) reached a maximum of ~20°C in June, remained near this level until October, decreased to a minimum of ~5°C in January, and then increased. Similar to the temperature, the relative humidity (RH; Figure 2) also showed large seasonal variations, indicating two distinct environmental conditions (dry and wet), with consequences for aerosol microphysical and optical processes. During the dry months (December–March), the ambient humidity remained below 50%, with a slight increase in January. The daily

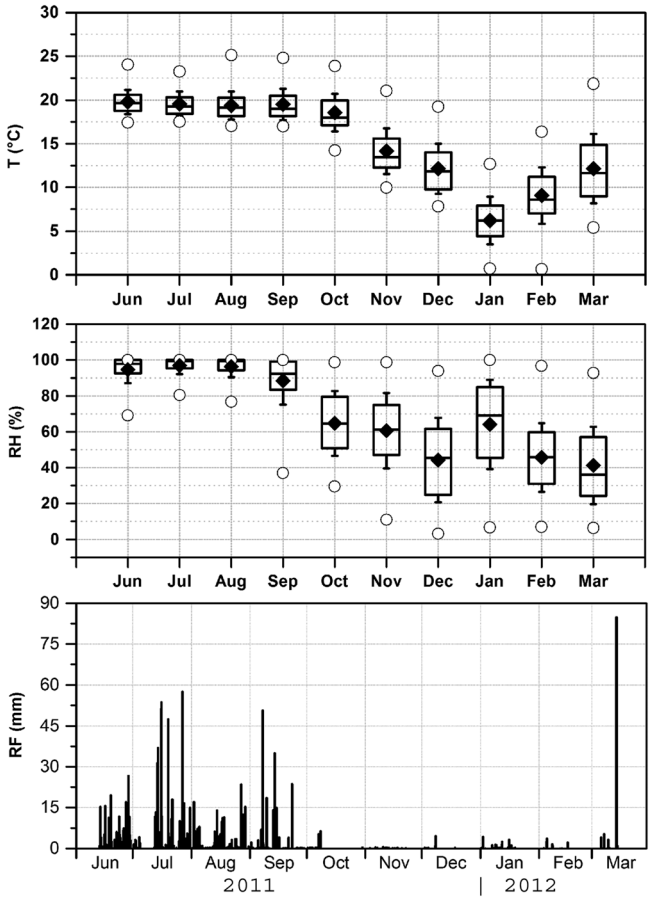

Figure 2. Variation of monthly mean temperature (T, in °C; top), relative humidity (RH, in %; middle), and daily total rainfall (in millimeter; bottom) during the measurement period, showing two distinct ambient conditions.

total rainfall (RF; Figure 2) reached a maximum of 57 mm during the monsoon season. During autumn (September–November) and winter, the daily total rainfall was lower (<10 mm).

3. Instrumentation and Analysis

All aerosol measurements and supporting meteorological data from the AMF instruments were obtained according to the AMF protocols [*Jefferson*, 2011]. We used the following data for this study:

1. *Integrated angular scattering* (σ_{sca}) *and hemispheric backscattering* (σ_{bsc}) *coefficients* at 450, 550, and 700 nm for particle sizes <1 μm and <10 μm, as measured by an *integrating nephelometer* (TSI 3563). The sample was controlled at a RH of 40% to measure the properties of the intrinsic dry aerosols with minimal contribution from water and to minimize the evaporation of semivolatile organics and acids from the aerosols.
2. *Aerosol absorption coefficients* (σ_{abs}) at 467, 530, and 660 nm for particle sizes <1 μm and <10 μm, as measured by the *particle soot absorption photometer* (PSAP; Radiance Research).
3. *Aerosol number density* (#CN) for particle diameters of 10 nm to 3 μm, as measured with a CN *counter* (TSI 3010).
4. *Cloud condensation nuclei number density* (#CCN) at six SS levels, as measured with a *CCN counter* (single-column Delft Mass Transport model release 1).

The Nephelometer and PSAP data collections were preceded by two switched impactors with size cuts at 10 μm and 1 μm. The 10 μm impactor removes particles with aerodynamic diameters >10 μm, while the 1 μm impactor removes supermicron particles. Every 30 min, the sampling switches between the 10 μm and 1 μm impactors.

3.1. Nephelometer Measurements

Nephelometer measurements of aerosol scattering coefficients (σ_{sca}) are obtained by illuminating a fixed volume of a sample from the side and counting the electronic pulses of the photons scattered by particles and gas molecules in the sample volume in the direction of a photomultiplier tube. The TSI nephelometer integrates σ_{sca} over angles of 7°–170° and backscattering coefficients (σ_{bsc}) over angles of 90°–170°. We followed the methods of *Anderson and Ogren* [1998] to correct the angular nonidealities (i.e., truncation) of the nephelometer raw data. Other uncertainties include instrument noise and the calibration drift (which is <10 M m^{-1} for σ_{sca} ~100 M m^{-1}). For submicron aerosols, the uncertainty associated with the inlet tubing is insignificant. Particle losses inside the nephelometer volume are negligible for submicron particles and are 5–10% for supermicrometer particles [*Anderson and Ogren*, 1998]. The uncertainty in particle transmission through the submicron impactor is <5%, depending on the particle type, and is influenced by the effect of the RH on the particle size. The flow rate uncertainty in the nephelometer is within 1–2% of the

expected range. The nephelometer was calibrated periodically using CO_2 as a high-span gas (which has a high scattering coefficient) and air as a low-span gas (which has a low scattering coefficient).

3.2. PSAP Measurements

A PSAP monitors the particulate absorption due to changes in the transmission of light-emitting diode radiations at 467, 530, and 660 nm (for a three-wavelength system) or at 550 nm (for a single-wavelength system) across a fibrous glass filter. The absorption coefficient is calculated from the amount of light absorbed, the area of the filter, and the volume of air sampled. We followed the method of *Virkkula* [2010] to analyze the raw PSAP data and estimate the true aerosol light absorption coefficients; the flow and spot size calibrations were incorporated. The nonlinear response of the unit due to the filter load was accounted for by following an empirical calibration procedure. Additional biases arise due to scattering aerosols, loading multiple samples onto the filter medium, the variability in each PSAP unit and instrument noise (~6% of the total absorption [*Bond*, 2001]). From the intercomparison of filter- and photoacoustic-based aerosol light absorption measurements on board the NOAA research vessel *Ronald H. Brown* in the Gulf of Mexico and inland water near Houston, *Lack et al*. [2008] have reported that PSAP noise and uncertainty increase in high-RH environments and in air with high concentrations of semivolatile organics. This finding is attributed to the (a) modification of the filter surface and subsequent light scattering and (b) the possible coating and absorption enhancement of preexisting absorbing particulate matter (PM, i.e., soot) due to the deposition and redistribution of liquid-like organic PM around the fiber filters.

3.3. Spectral Index of Scattering and Absorption

The spectral dependence of σ_{sca} can be used to delineate the domination of accumulation (size <1 μm) or coarse-mode (>1 μm) aerosols. Similarly, the spectral variation in σ_{abs} is indicative of the presence of aerosol species other than BC (such as organic carbon (OC) and dust) that strongly absorb short wavelengths (blue and ultraviolet) [*Kirchstetter et al*., 2004]. Approximating the wavelength variation in the scattering and absorption coefficients by an inverse power law similar to the Ångström equation (equation (1)), the wavelength exponents of α_{sca} and α_{abs} were determined for each measurement of the nephelometer and PSAP.

$$\sigma = \beta\lambda^{-\alpha} \tag{1}$$

where σ and α correspond to the coefficients and wavelength indices, respectively; subscript "sca" denotes the scattering (σ_{sca} and α_{sca}) and "abs" denotes the absorption (σ_{abs} and α_{abs}).

3.4. Total Condensation Nuclei Measurements

The Model 3010 CN counter (TSI) detects particles with diameters >10 nm. The particles are allowed to grow into droplets in the presence of condensing alcohol vapor before they are counted with a simple optical particle detector. The SS ratio of the fluid vapor in the condenser controls the minimum detectable particle size range of the counter.

The local contamination issues that influence the CN concentrations were negligible at Nainital given that the observation site is ~ 2 km above mean sea level, which is well above the mixed layer; therefore, the relatively clean environment was free of local pollution, and the aerosol characteristics closely resemble those of the free troposphere. When the data set was contaminated by local activities, such as vehicle movement or activities near observatories, the anomalous values were easily identifiable in the time series plot and were excluded prior to the data set analysis.

3.5. Cloud Condensation Nuclei Measurements

The CCN counter measures the activated particle concentration, that is converted to cloud droplets by condensation at a given SS. At Nainital, the SS settings for the CCN counter progressed over six 5 min settings every 30 min. Because the instrument column thermal properties add small variations to SS, we followed the procedure of *Jefferson* [2011]; accordingly, the first minute of data at every SS setting was disregarded because of the unstable CCN temperature, and only the last 4 min of data were averaged for the analysis. For a given diameter and SS, the CCN activity was reported as the AR: the ratio of the number of particles that act as CCN to the total number of CN counted by the CN counter.

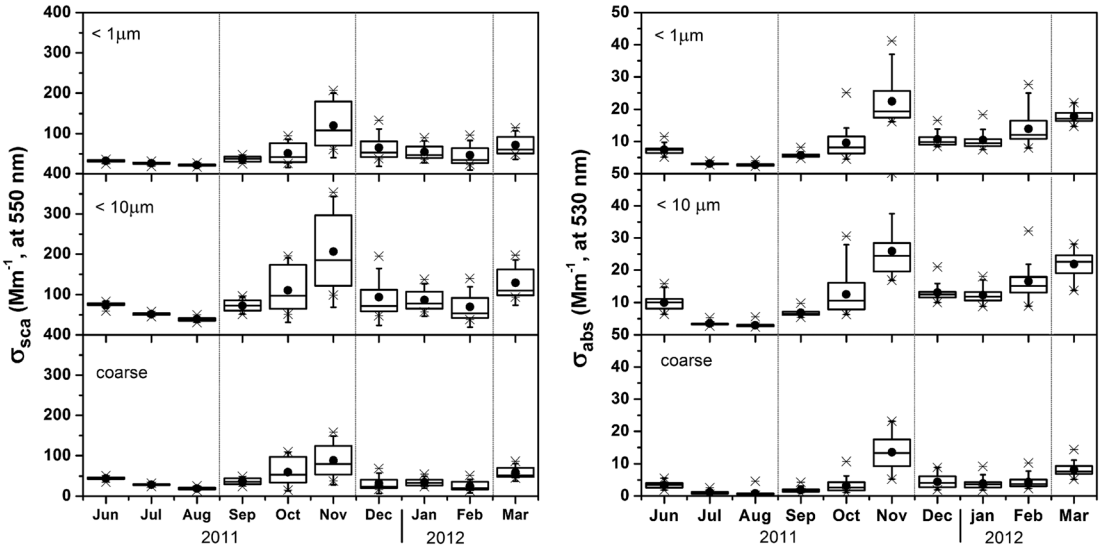

Figure 3. Temporal variation of monthly average aerosol scattering (at 550 nm) and absorption (at 530 nm) coefficients. The monthly means (black square), standard deviations (vertical bars), 25th percentile (lower dash line), median (middle dash line), and 75th percentile (top dash line) occurrences and the monthly minimum and maximum hourly mean values (cross sign) are shown. Aerosol regimes are (top) <1 μm, (middle) <10 μm, and (bottom) 1–10 μm (coarse).

The CCN instrument was serviced and calibrated at the beginning of the deployment for the mobile facility at Nainital. The following were calibrated:

1. supersaturation rate;
2. main flow, CCN sheath, and sample flows;
3. CCN pressure; and
4. optical particle counter.

Per the ARM protocols, the high-efficiency particulate air filters, mass flowmeter, and pump diaphragm were replaced before deployment, a bleach solution was used to purge the CCN column, the capillary sample tube and inlet line were cleaned, and any leakage of CCN was checked during periodic maintenance.

4. Results and Discussion

4.1. Scattering and Absorption Coefficients

Aerosol scattering and absorption coefficients (σ_{sca} and σ_{abs} at 550 nm and 530 nm, respectively) are shown in Figure 3 for the temporal variation in the monthly average values for aerosol regimes <1 μm (Figure 3, top), <10 μm (Figure 3, middle), and between 1 and 10 μm (coarse mode; Figure 3, bottom). In all of the cases, both σ_{sca} and σ_{abs} show large temporal variations, with the highest values toward late autumn (November) when the conditions are dry (autumn rainfall is ~14% of the annual total). The lowest values occurred at the end of the monsoon season (August). Rainfall is extensive during this season; the seasonal total rainfall accounts for nearly 68% of the annual total [*Dumka et al*., 2010; *Sagar et al*., 2004]. During winter (December–February), the values are low and increase into spring (March).

The aerosol single scattering albedo (SSA) at 530 nm derived from the nephelometer (interpolated to 530 nm using the estimated α_{sca} values) and PSAP measurements also show large annual fluctuations (Figure 4), with the monthly mean values of 0.76 ± 0.04 to 0.86 ± 0.03 for aerosols <1 μm and 0.79 ± 0.04 to 0.90 ± 0.02 for aerosols <10 μm. The monthly variations in the SSA indicate a relatively higher fraction of aerosol absorption in the dry autumn and winter (SSA < 0.80) and a relatively stronger scattering fraction of aerosols (SSA > 0.85) during the monsoon season.

On the basis of time series analyses of bulk aerosol samples collected at Nainital with a high-volume sampler, *Ram et al*. [2008] have reported that the relatively high abundance of total suspended particulates during April–June is associated with enhanced contributions from mineral dust when both organic carbon and

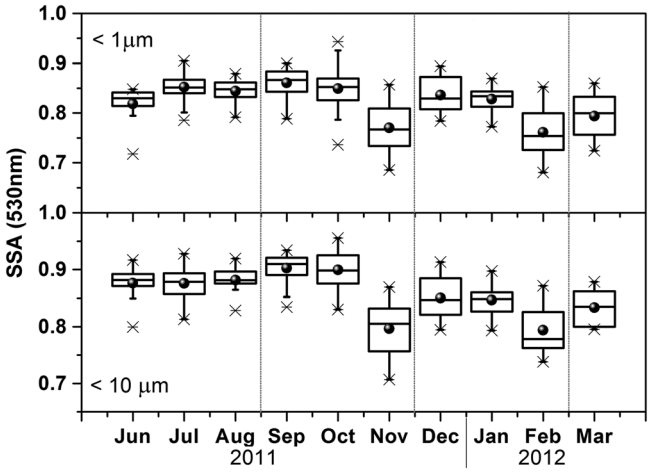

Figure 4. Temporal variation of monthly average aerosol single scattering albedo at 530 nm. The error bars indicate the standard deviation. The dash lines indicate the 25th percentile (lower line), median (middle line), and 75th percentile (top line) occurrences.

elemental carbon abundances are at a minimum. In contrast, a characteristic dominance of carbonaceous species (both organic and elemental) has been reported in autumn and winter. To examine the seasonality of scattering or absorbing aerosols, the monthly variations in α_{sca} and α_{abs} are shown in Figure 5 for both the <1 μm and <10 μm particle size regimes. Higher values of α_{sca} (approximately 2) correspond to situations when accumulation-mode particles <1 μm contribute to scattering. An abundance of coarse-mode particles (size >1 μm) results in a decreased steepness of the spectral response of scattering coefficients [e.g., *Seinfeld and Pandis*, 1998]. However, the higher spectral dependence of the absorption coefficient (α_{abs}~2.0) indicates a dominance of biomass burning or dust aerosols [*Kirchstetter et al*., 2004; *Bergstrom et al*., 2007], whereas the presence of fossil fuel combustion is indicated by values of α_{abs}~1.0. From a study of optical and chemical properties of aerosols in Northeast Asia, *Lee et al*. [2010] have reported that α_{sca} varies from 0.8 to 1.8 for scattering due to sulfate, nitrate, ammonium, and carbonaceous aerosols (fine particles), whereas relatively high values of α_{abs} (~1.0–1.5) are noted for spectral absorption by refractory organic carbon in the near-ultraviolet region. Case studies from various field programs [e.g., *Bergstrom et al*., 2007] also indicate that the spectral variation in aerosol absorption changes from α_{abs}~1 for urban pollution to α_{abs}~2 for biomass smoke, with larger values (α_{abs}~3) for dust aerosols.

In the present study, α_{sca} and α_{abs} showed large seasonal variations for aerosols <10 μm and <1 μm (Figure 5). The monthly variation in α_{sca} for aerosols in the <10 μm size regime indicates that the relative dominance of coarse aerosols (α_{sca}~0.81) was high in June and November and it built up toward the end of winter, as indicated by the minimum value of α_{sca}~0.75 in March. For aerosols in the <1 μm size range, the seasonal variations in α_{sca} were similar to those for aerosols <10 μm, indicating the dominant signature of larger-sized particles in June, November, and March. The size dependence of scattering during the study period at Nainital has been discussed in detail by *Manoharan et al*. [2014]. From the gravimetric analysis of total suspended particulate (TSP) mass at Nainital, *Ram et al*. [2010] have reported that the higher TSP mass during April–June

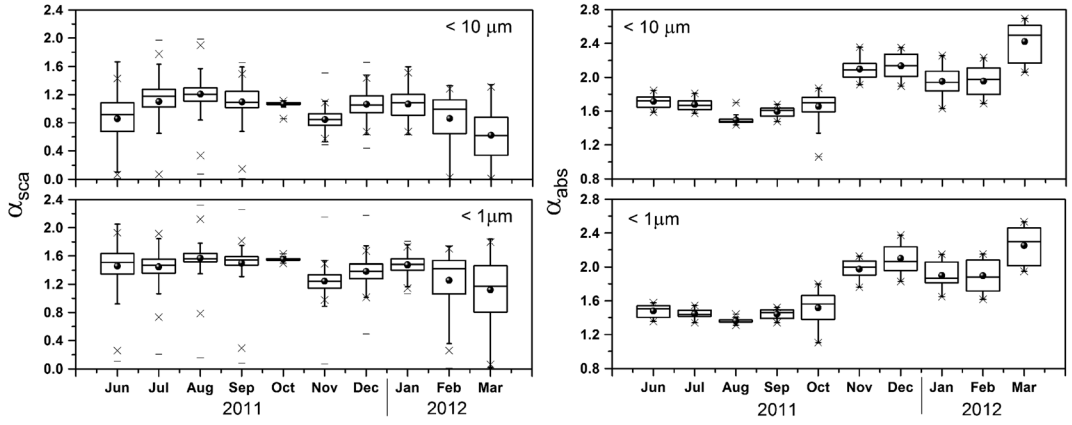

Figure 5. Temporal variations of (left) α_{sca} and (right) α_{abs} for aerosols (top) <10 μm and (bottom) <1 μm size regimes, June 2011–March 2012.

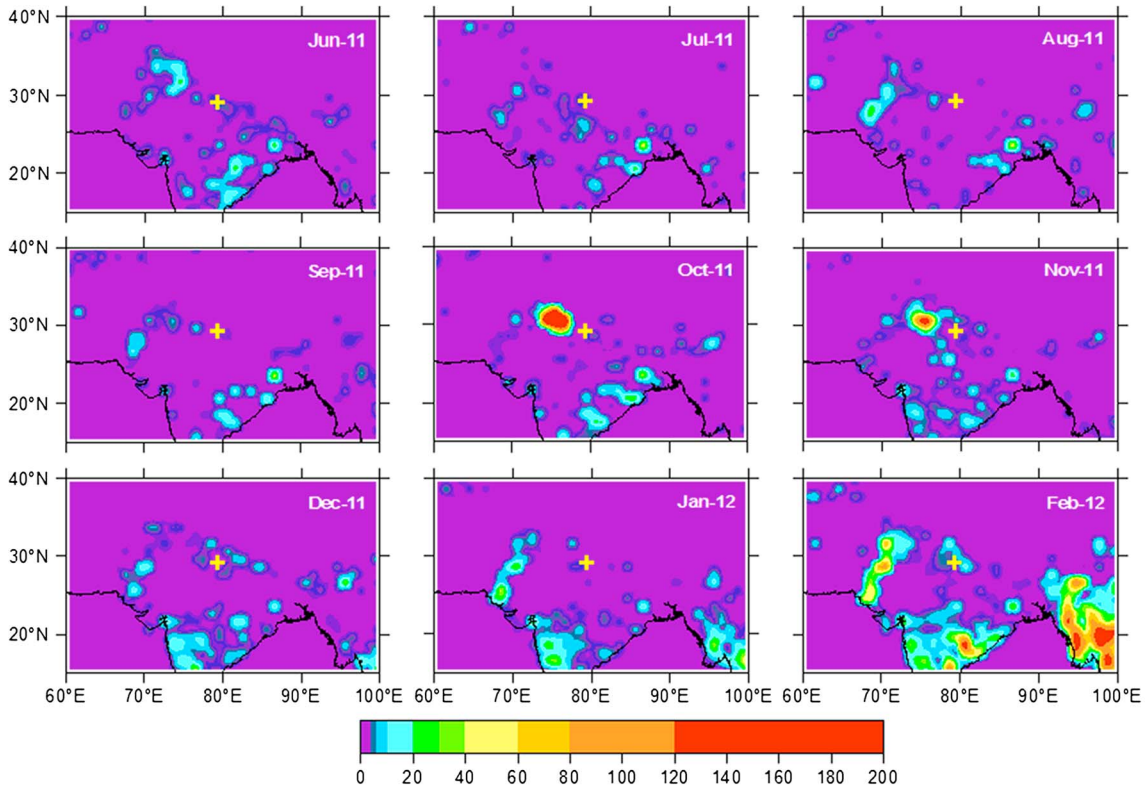

Figure 6. Spatial distribution of MODIS cloud-corrected fire pixel counts for each month of different seasons during the study period. The geographic position of Nainital is shown by the plus sign.

arises from the dominant contribution of mineral dust (transported from the Thar Desert (in western India) and the Middle East), as evident from an increase in the concentrations of carbonate carbon and calcium ions (Ca^{2+}). Additionally, higher-humidity conditions during the monsoon may contribute to the flatter wavelength dependence, as the hygroscopic growth of aerosols tends to flatten the size spectrum.

In the case of α_{abs}, the systematic variations shown in the Figure 5 (right) are indicative of the relatively higher contribution of biomass-burning aerosols during November–March ($\alpha_{abs} \geq 2.0$) compared with June–October ($\alpha_{abs} < 1.8$) for both $<10\,\mu m$ and $<1\,\mu m$ particles. Based on a long-term (2005–2008) study of the chemical composition and optical properties of aerosols from the same experimental site at Nainital, *Ram et al.* [2010] have reported that relatively high concentrations of OC and elemental carbon (EC) occur during the postmonsoon and winter months (November–March). The authors have reported that the highest monthly mean OC concentrations occur in October ($12.2 \pm 6.3\,\mu g\,m^{-3}$). High OC and EC are also reported over Kathmandu (in the eastern Himalayas) during the postmonsoon and dry months [*Adhikary et al.*, 2007]. However, regions dominated by biomass-burning aerosols depict a higher ratio of OC to EC (OC/EC). The higher OC/EC ratio (7.5 ± 1.3) at Nainital during the postmonsoon (autumn) period is indicative of the contribution from organic aerosols associated with the transport of biomass-burning emissions in the IGP and western India [*Ram et al.*, 2010]. As shown in Figure 6, this finding is corroborated by satellite fire counts, indicating the presence of organic components during autumn and winter, consistent with the observations of *Ram et al.* [2010].

4.1.1. MODIS Fire Counts

To support the above-mentioned seasonal features of aerosol spectral absorption, the spatial distribution of Moderate Resolution Imaging Spectroradiometer (MODIS) cloud-corrected fire pixel counts is examined (Figure 6). We used the Climate Modeling Grid Fire Product (MOD14CMH) at a 0.5° spatial resolution for a time period of one calendar month. The fire detection algorithm considers land pixels (after excluding the cloud and water masks) as "fire pixels" if one or more fires are actively burning at the time of the satellite overpass [*Giglio et al.*, 2006]. The area of a pixel is nominally 1 km^2 at nadir. Figure 6 shows a large area to the west of

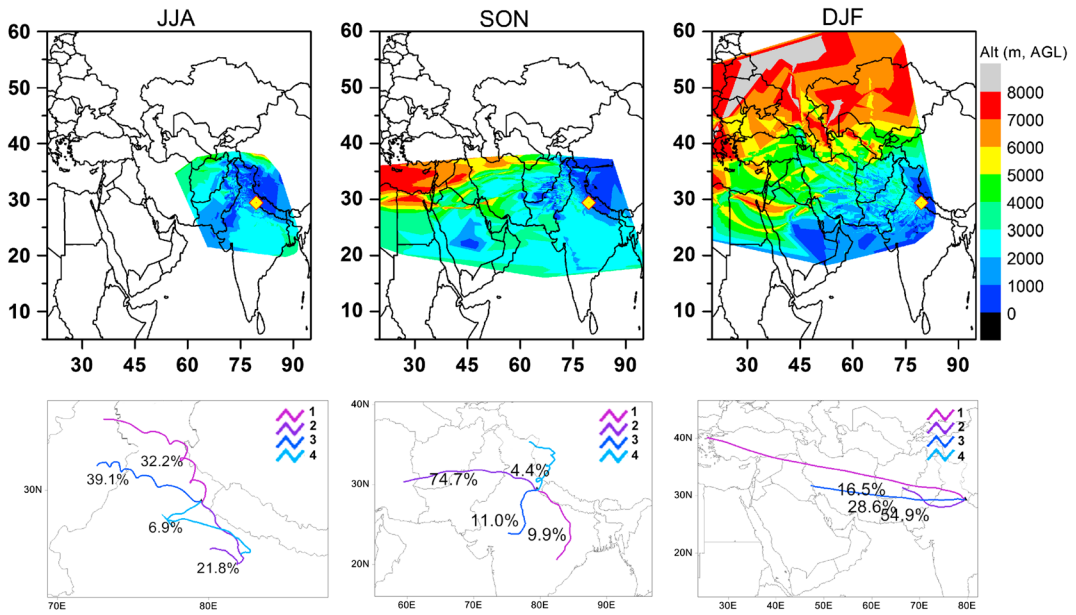

Figure 7. (top) Isentropic air mass back trajectories ending at 500 m aboveground level at Nainital (yellow diamond) in monsoon (JJA, June-July-August), autumn (SON, September-October-November), and winter (DJF, December-January-February), with colors (right bar) showing the altitude variation of trajectories during traversal of distant locations and (bottom) trajectory clusters in the three seasons.

Nainital covered by intense burning activities during late autumn (October and November) and toward the end of winter (February). Thus, the gradual increase in the steepness of the spectral absorption (indicated by α_{abs} in Figure 5, right) from the monsoon to the dry autumn and winter arises from the increasing contributions of enhanced biomass-burning aerosols. *P. Kumar et al.* [2011] have reported that crop residue burning activity over northern India, including the central Himalayan region, was highest during spring (March, April, and May) and significant during autumn (September, October, November). The high density of MODIS fire locations over cropland areas west of Nainital, as reported by *P. Kumar et al.* [2011], is consistent with the dominance of agricultural fires, as reported by *Venkataraman et al.* [2006]. These observations, along with the results of the aerosol chemical composition reported by *Ram et al.* [2010], could explain the high spectral aerosol absorption coefficients apparent during autumn and toward the beginning of spring. Notably, dust also has strong absorption at shorter wavelengths, particularly IGP dust, which is iron rich [*Kumar et al.*, 2010]. Although biomass-burning aerosols are dominant in autumn, dust would also contribute to the reduced SSA during this period. As already mentioned, the presence of dust in autumn (November) is evident from the lower Ångström coefficients for scattering, suggesting greater coarse-mode particle abundance in the aerosol size spectrum.

4.1.2. Air Mass Patterns

Five-day isentropic air mass back trajectories (from Hybrid Single-Particle Lagrangian Integrated Trajectory (HYSPLIT) modeling) ending 500 m aboveground level at Nainital (Figure 7, top) clearly show significant seasonality in trajectory pathways and altitudes. During the monsoon season and autumn, significant air mass contributions arrive from mainland India, as indicated by the contributions of the trajectories in each cluster (calculated according to *Gogoi et al.* [2013]) shown in Figure 7 (bottom). Conversely, the trajectories originating from the Indian subcontinent are insignificant during winter. During the monsoon, the trajectories are mostly confined to lower altitudes (<3 km), as shown in Figure 7 (top left), and smaller regions than in autumn and winter. During autumn, even though large numbers of trajectories reside at lower altitudes (<3 km), the trajectories originate at much higher altitudes (>7 km) at distant western locations. During winter, all of the trajectories cover a large area and mostly originate at high altitudes. These observations indicate that synoptic conditions are favorable for dust transport during the monsoon season and autumn, while winter conditions are dominated by fine-mode aerosols. However, the higher absorption by aerosols during autumn and winter is associated with the traversal of air masses over fire-impacted regions before they reach Nainital [*P. Kumar et al.*, 2011].

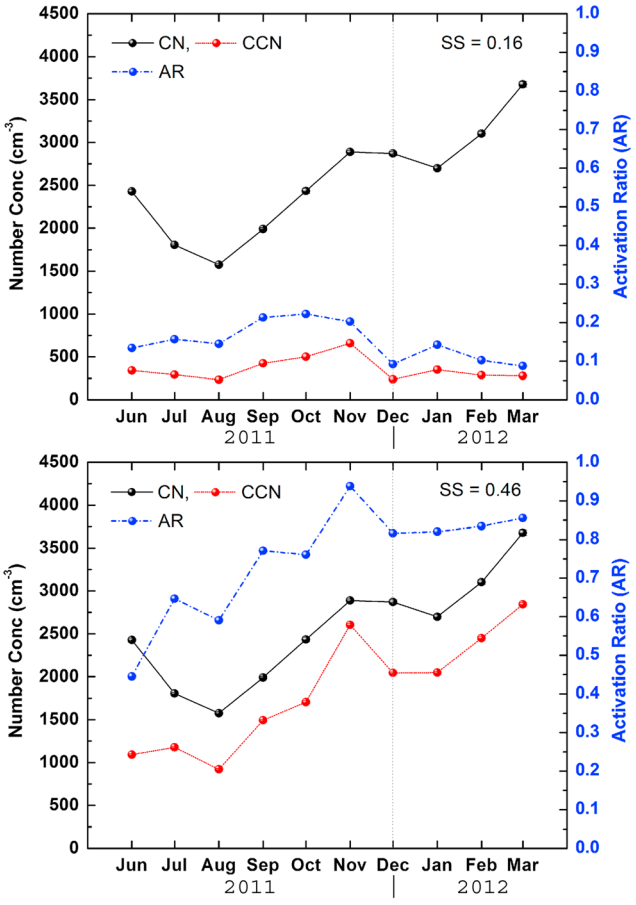

Figure 8. Monthly variations of CN and CCN at two specific SS (SS = 0.16 and SS = 0.46), along with the monthly mean values of the CCN activation ratio (AR) at SS = 0.46.

4.2. Aerosol CCN and CN Concentrations

After characterizing the optical properties of aerosols, we examined the characteristics of CCN activity at Nainital. Figure 8 shows the monthly variations in the CCN concentrations and their activation ratios (ARs = CCN/CN) at two distinct SSs (0.16 and 0.46). Note that a SS of 0.46 is representative of convective clouds, which have dynamic feedback due to changes in CCN; however, these clouds are less susceptible to cloud albedo changes due to changes in CCN. Large-scale stratus clouds are most susceptible to albedo changes due to changes in CCN at a maximum supersaturation of 0.1–0.2% [*Pierce and Adams*, 2009]. It is seen that CCN concentrations and the respective ARs at a low SS (0.16) do not generally show significant seasonal changes, but they are slightly higher during autumn (September through November). However, at a higher SS (0.46), a remarkable change occurs in the monthly variation in CCN concentrations, with increased CCN concentrations in autumn (highest in November) and winter. The monthly mean CN concentrations (plotted along with the CCN concentrations and AR in Figure 8) are clearly enhanced in the dry autumn and winter and are highest in March (CN~3697 ± 2367 cm^{-3}) of the study period. Thus, the higher CCN concentrations in winter are mainly due to the higher concentrations of CN. However, the AR is highest toward the end of autumn (November) even though the CN concentrations are higher in winter.

To examine the variation in the CCN at all of the SS levels, we segregated the CCN concentrations at different SS values and plotted the monthly mean values as a function of SS, as shown in Figure 9. In all seasons, the CCN concentrations generally increased as SS increased, but the variations were less sharp during the monsoon season than during autumn or winter. During the monsoon, even with the gradual increase in the CCN concentrations as the SS increased, the variations became nearly stable beyond SS~0.4. However, the CCN concentrations increased by an order of magnitude during autumn (from 247 to 2473 cm^{-3}) and winter (from 131 to 2690 cm^{-3}) as the SS changed from 0.1 to 0.7. Therefore, the fraction of CN that serves as CCN is much lower during the monsoon season. The differences between monsoon and winter are minimal and are within the uncertainty range of the CCN measurements below a 0.2% supersaturation. At a high-altitude location such as Nainital, which is devoid of any major local source effects, the change in the aerosol types is mainly governed by the long-range transport of aerosols.

In general, an increase in the relative abundance of hygroscopic particles in a given aerosol system increases the CCN formation ability. However, insoluble matter can also affect the activation. *Fletcher* [1962] proposed a theory of water nucleation on insoluble spherical particles with uniform surfaces. Similarly, a mixture of soluble substances and a partially hygroscopic insoluble core can also lead to cloud droplet formation [*Gorbunov and Hamilton*, 1997]. *Twohy and Anderson* [2008], *Dusek et al.* [2006], *Junge and McLaren* [1971], *Fitzgerald* [1973], *Pruppacher and Klett* [1978], and *Harrison* [1985] have found that both aerosol size distributions and chemical compositions govern CCN activation. According to the Köhler equation, the SS

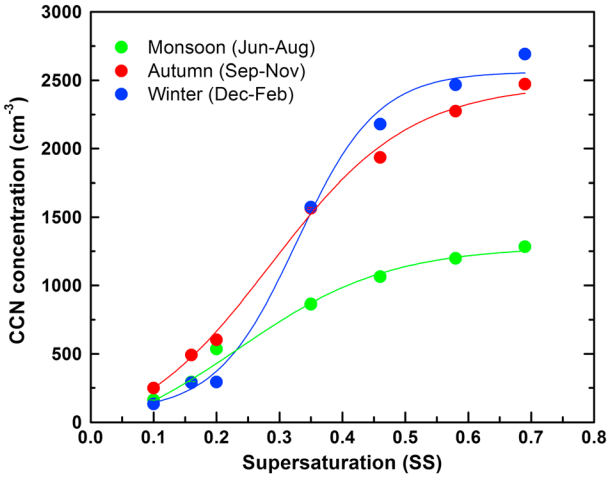

Figure 9. Variation of monthly mean CCN concentration with respect to mean SS (in each setting) in monsoon (JJA, June-July-August), autumn (SON, September-October-November), and winter (DJF, December-January-February).

of an aqueous drop varies with the drop surface tension or size and the solute concentration or chemical composition. As SS increases, the CCN concentration also increases because a higher SS leads to the activation of smaller and less hygroscopic or insoluble particles under particular conditions. Thus, the high CCN concentration and near-unity AR (Figure 8) above a 0.5% supersaturation during autumn and winter are indicative of the CCN activation of most of the smaller particles. In contrast, the AR for the monsoon period nearly levels off at 0.6–0.7 for a supersaturation >0.5%, suggesting that a significant fraction of CN remain unactivated, probably because they are far less hygroscopic, or even hydrophobic, in nature.

To examine the activation efficiency of CN that form CCN at different SSs, the seasonal mean AR at different SSs are plotted in Figure 10 for three distinct seasons: monsoon, autumn, and winter. During the monsoon season, the AR increases steadily with an increase in SS but levels off and remains below 0.7 (even at the highest SS). However, the fractional contribution of CN to CCN (i.e., AR) during the dry autumn and winter is higher than that in the wet monsoon season, reaching a stage of near-complete activation at very high SS.

Setting our study in a global framework, Table 1 lists the CN and CCN concentrations and the values of AR (CCN/CN) measured at other high-altitude or urban/polluted locations, including those reported from observational data collected at multiple ARM sites (Graciosa (GRW), Niger (NIM), Oklahoma (SGP), and Black Forest (FKB)). At Graciosa Island (GRW) in the Azores, even though the concentrations of CN and CCN at 0.4 SS are low and associated with sparse anthropogenic activities, the CCN AR is high [*Liu and Li*, 2014]. The moderately high CCN concentration (at 0.4 SS) reported for the NIM site is due to the high CN concentrations associated with frequent dust events. However, the AR at NIM is minimal, indicating a reduced activation efficiency of dust at any given SS. Our results are similar to those reported at GRW for autumn and winter with a high AR, whereas the low AR during the monsoon season is similar to that reported for NIM. The higher AR at Nainital during autumn and winter can also be attributed to the dominant westerly advection, which transports a large fraction of mix-phased aerosols that act as CCN at high SS. Additionally, the measurement site at Nainital occasionally resides above the boundary layer mixing height, particularly in autumn and winter; thus, additional aged aerosols in the free tropospheric region contribute to the high AR during these seasons. Compared with other high-altitude sites, the CCN concentrations at Nainital are high compared with those at Jungfraujoch (3580 m asl), even though the ARs at Jungfraujoch are more variable due to a greater variability in the total particle concentration and the effects of physical (e.g., shape and size distribution) and chemical properties. Compared with several

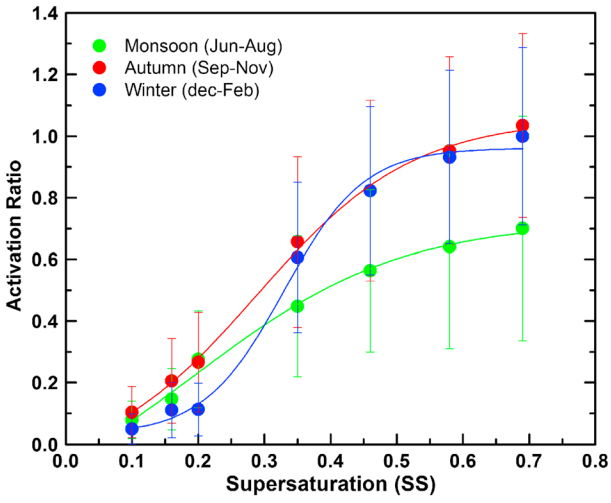

Figure 10. Variation of mean AR with SS in different periods of monsoon, autumn, and winter.

Table 1. CCN, CN, and Activation Ratio (CCN/CN) at Nainital and Those Reported Over Other High-Altitude and Urban/Polluted Locations

Location	Period	#CCN (cm^{-3})	#CN (cm^{-3})	Activation Ratio (AR = CCN/CN)	Reference
		High-Altitude Sites			
Nainital (1958 m), India	Jun 2011 to Mar 2012	1838.23 (mean)	2,548.03 (mean)	0.74 at SS = 0.46	Present study
	JJA (monsoon)	1063.59 ± 10.39	1,936.81 ± 440.53	0.56 at SS = 0.46	
	SON (autumn)	1935.44 ± 14.46	2,438.48 ± 448.65	0.82 at SS= 0.46	
	DJF (winter)	2180.14 ± 16.05	2,891.44 ± 202.42	0.82 at SS = 0.46	
Graciosa (GRW), Azores	May 2009 to Dec 2010	287 ± 263	615 ± 587	0.53 ± 0.30 at SS = 0.4	*Liu and Li* [2014]
Niger (NIM)	Aug 2006 to Jan 2007	726 ± 780	5,561 ± 5,476	0.20 ± 0.24 at SS = 0.4	
Southern Great Plains (SGP), Oklahoma	Sep 2006 to Apr 2011	1248 ± 896	3,944 ± 2,992	0.40 ± 0.24 at SS = 0.4	
Black Forest (FKB), Germany	Apr 2007 to Dec 2007	1007 ± 749	3591 ± 2,098	0.29 ± 0.17 at SS = 0.4	
Jungfraujoch (3580 m), Switzerland	May 2008	149 ± 171 at SS = 0.12 568 ± 401 at SS = 1.18	550	0.2–0.8 at SS = 0.47	*Juranyi et al.* [2010]
		Urban/Polluted			
Vienna, Austria	Jul 2007 to Oct 2008	820 at SS = 0.5	7,300	0.13 at SS = 0.5	*Burkart et al.* [2011]
Guangzhou, southern China	Jul 2006	9649 ± 5214 at SS = 0.47	18,150 ± 7,991	0.53 ± 0.19 at SS = 0.47	*Rose et al.* [2010]
		Background Locations			
SMEAR II station, Hyytiala, Finland	Jul 2008 to Jun 2009	546.5 ± 194.3 at SS = 0.4		0.34 ± 0.06 at SS = 0.4	*Sihto et al.* [2011]
Arctic	Jun–Jul, 2008	247 at SS = 0.55	514	0.52 at SS = 0.55	*Lathem et al.* [2013]

urban/polluted regions dominated by anthropogenic emissions, the CCN activity greatly differs at Nainital, where the CN and CCN concentrations are much lower. However, the AR at Nainital is comparable to that seen at some of the urban sites. Compared with the results at a pristine location, such as the Arctic, the CCN concentration and the AR at Nainital are definitely higher. The variations in the CCN concentration at pristine sites are due to variations in the CN concentration and differences in the size distribution and chemical composition.

Lathem et al. [2013] have reported that the higher CN and CCN concentrations over spatially extensive regions at 50°–60°N are due to biomass burning and industrial emissions that increase the concentrations by 1–2 orders of magnitude over background levels. *Dusek et al.* [2006] have reported that SS values in the range of 0.25–1.5 are conducive for activating particles of any composition, but sizes >0.12 μm, as CCN; however, unrealistically high SS values are required for the activation of much smaller particles (<40 nm). For aged background aerosols (particles sizes >50 nm), a 1% SS can lead to complete activation (AR~1), while the AR at the same SS is quite low for fresh (e.g., urban) aerosols [*Andreae and Rosenfeld*, 2008]. Examining the results at Nainital based on the above reports, it appears that the higher CCN AR at Nainital during the dry months arises from aged background aerosols mixing with advected biomass-burning aerosols.

The above discussion on the variations in the ARs and the concentrations at different locations and seasons helps understand the CCN characteristics at Nainital and the variations in aerosol types caused by synoptic meteorological conditions, which play a major role in activating aerosols. The findings are generally consistent with the observed optical properties of aerosols and their associations with distinct sources and transport processes in different seasons.

Figure 11 shows the monthly variation in the correlation coefficients of the CCN concentrations with the simultaneous values of σ_{sca} and σ_{abs} for the size regimes of <10 μm (open black circle) and <1 μm (filled green circle). A strong correlation (≥0.85, except in October) between the CCN concentrations and σ_{sca} is observed for the accumulation-mode size regime (<1 μm) during most of the study period. The coarse-mode fractions (CMF; size >1 μm) of σ_{sca} (at 550 nm) for various months are also shown in the figure (red dotted line in Figure 11, top), along with the monthly mean values of AR. Clearly, the contribution of coarse-mode aerosols (>1 μm) to the total scattering (i.e., CMF) is higher (>0.38) in June–October than in other seasons, notwithstanding the high rainfall during the monsoon season. The monthly mean values of the AR (for SS = 0.46) generally follow a pattern that is nearly opposite that of the CMF of scattering aerosols. For example, the lowest AR is associated with a higher CMF in June 2011, whereas the AR is nearly stable when the CMF increases from December 2011 to March 2012. This observation clearly indicates

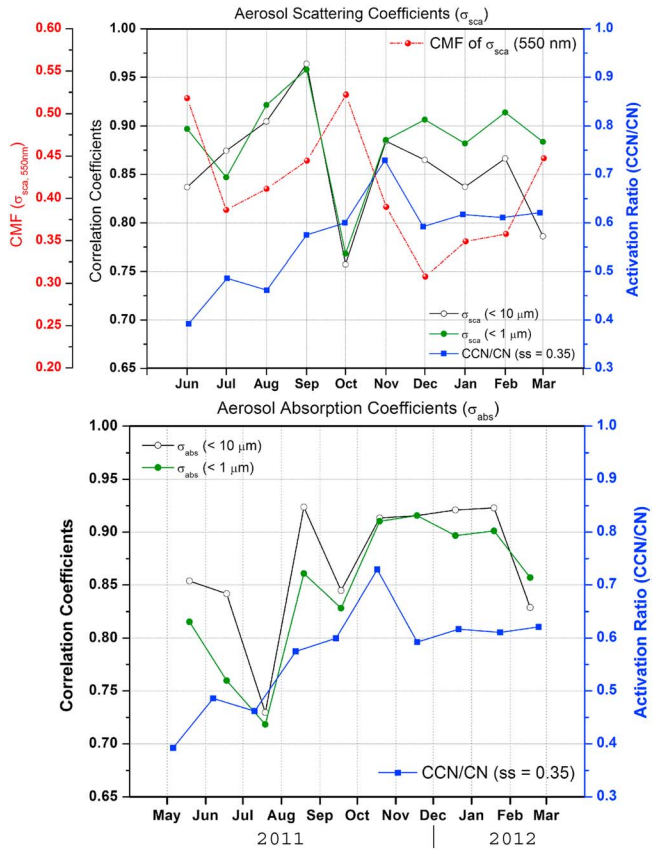

Figure 11. Monthly variation of correlation coefficients (R^2) of CCN concentrations (at SS = 0.35) with (top) σ_{sca} and (bottom) σ_{abs} for both size regimes of <10 μm (open black circle) and <1 μm (filled green circle), along with coarse-mode aerosol fraction (>1 μm) to total scattering at 550 nm (red dotted line in left). The monthly mean AR is shown by the blue lines with respect to right *y* axis in both panels.

the prevalence of dust aerosols in June 2011 that are not activated. The prevalence of dust over the IGP and Nainital during May–June has also been independently reported [*Hegde et al*., 2007; *Dipu et al*., 2013; *Ram et al*., 2010; *Kumar et al*., 2014].

However, the abundant biomass-derived aerosols with $\alpha_{abs} > 1.8$ might be activated as CCN under favorable meteorological conditions during autumn and winter. This finding is clearly reflected in November, when the AR is highest and a strong correlation exists between the CCN and σ_{abs} for the fine-mode regime. Although the correlation of the CCN concentrations with scattering aerosols is high in November, the seasonal variation in the aerosol SSA (shown in Figure 4) indicates a relatively higher fraction of absorbing aerosols during autumn (low SSA) when the aerosol AR is higher. The relationships between the aerosol SSA (Figure 4) and the AR (Figure 11) indicate that despite the relatively higher dominance of the absorbing fraction of aerosols (SSA < 0.8), higher CCN ARs prevail in autumn and winter than when the scattering fraction of aerosols dominate (SSA > 0.85). A scatterplot of the simultaneous data sets of the CCN concentration and σ_{abs} of submicron aerosols (<1 μm) (Figure 12) lends further support to this concept, with the highest correlation observed in autumn ($R^2 = 0.93$).

Using the optical properties of aerosols measured at four ARM climate research facilities in Oklahoma (SGP), Black Forest (FKB), Hefei (HFE), and Graciosa (GRW) as proxies for the aerosol size and composition of CCN, *Jefferson* [2010] have presented an empirical model for estimating CCN concentrations at the four sites. CCN formation is weakly influenced by changes in the aerosol absorbing fraction or equivalent black carbon (EBC) at GRW and HFE. At GRW, the presence of highly hygroscopic sea salt moderates the influence of less hygroscopic aerosols such as BC. Even a small fraction of large sea salt aerosols may sufficient for activation at a low percentage of SS. However, dust moderates the influence of EBC at HFE. Interestingly, EBC and other organics have a strong influence on CCN formation at SGP and FKB. The empirical relationships thus reflect differences in the size-dependent aerosol composition at each site and their influence on CCN formation.

Several earlier investigators have also reported that because of their larger sizes and possible coating of organic compounds, biomass-burning aerosols are more likely to act as CCN than the finer BC particles from urban activities that involve fossil fuel combustion [e.g., *Schwarz et al*., 2008]. Aerosols from biomass burning act as CCN because they are primarily composed of organics. However, some of the CCN activity of biomass-burning aerosols may actually be due to co-resident inorganic constituents [*Leaitch et al*., 1996]. Although nascent BC aerosols are too small and insufficiently hydrophilic to contribute directly to CCN production, they eventually act as CCN after aging when they mix with soluble components (through condensation and coagulation) and undergo photochemical oxidation in the atmosphere [*Johnson et al*., 2008; *Semeniuk et al*., 2007; *Zhang et al*., 2008]. *Lammel and Novakov* [1995] and *Petzold et al*. [2005], based

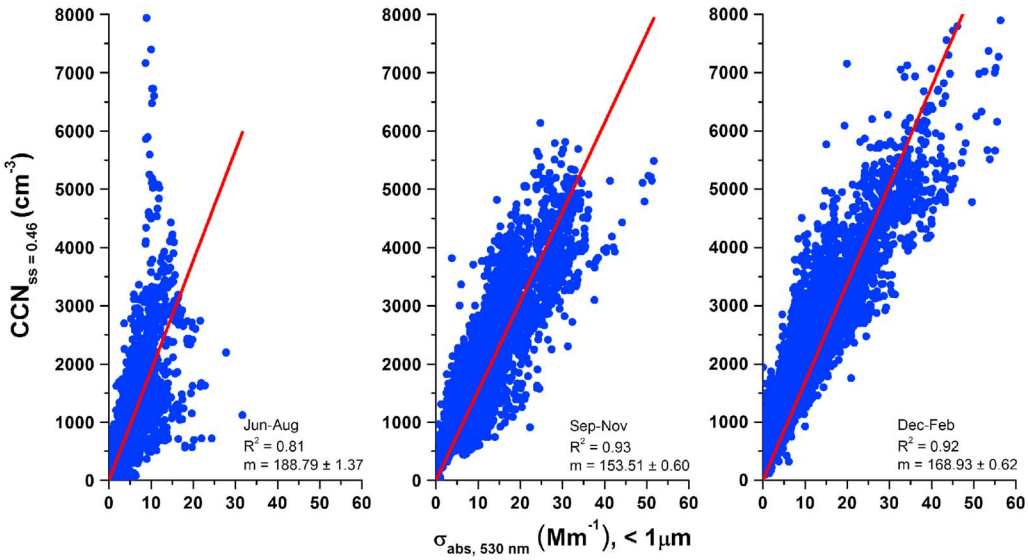

Figure 12. Scatterplot of CCN concentration (for SS = 0.46) against each set of absorption coefficients at 530 nm (for <1 μm particle size regime) at different seasons.

on laboratory investigations, have reported that BC particles are prone to activate as CCN because of the condensation of water-soluble organic compounds. The oxidation of aerosol particles over time also promotes CCN activation [*Furutani et al*., 2008; *Gao et al*., 2003]. All of the above factors appear to explain the high AR (Figure 11) during the dry autumn and winter at the high-altitude station of Nainital, which remains mostly above the planetary boundary layer during these months. Because the sources of absorbing aerosols at Nainital mostly originated at distant locations, the aerosols would age and would likely mix with other organic and/or inorganic materials that originate from biomass burning and with aged free tropospheric aerosols; the mixture would thus be amenable for more efficient activation, as has also been suggested by *Lee et al*. [2010] based on airborne in situ measurements.

However, mineral dust is a significant component of aerosols at Nainital during the spring and summer monsoon months [*Hegde et al*., 2007], but the dust aerosols are less hydrophilic and less active as CCN than common soluble salts [*Pruppacher and Klett*, 1978]. The dust at Nainital is mostly from distant sources, particularly western Asian and Indian desert regions. Mineral dust generated from windblown soil is amenable to long-range transport, particularly during the spring when wet removal is weak and convection is strong [*Bauer et al*., 2004]. Even in the summer, dust layers occur above the stratiform monsoon cloud systems. Mineral dust is a major contributor to the aerosol loading in Central India and the Himalayan region [e.g., *Moorthy et al*., 2007; *Hegde et al*., 2007]. However, as with BC, atmospheric processing in the presence of soluble nitrate or sulfate coatings could enhance the CCN activity of dust [*Gibson et al*., 2007]. In addition, dust could be coated and mixed with humic compounds and high-molecular-weight organics from biomass burning [*Russell et al*., 2002; *Falkovich et al*., 2004] that could enhance their hygroscopic properties [*Saxena et al*., 1995; *Wurzler et al*., 2000]. Cloud processing of these particles and interactions with preexisting hydrophilic particles mix the dust internally. Saharan dust particles have been reported to act as efficient ice nuclei [*Twohy et al*., 2009]. As a global average, particularly at remote locations, aerosol species are believed to undergo several condensation-evaporation cycles [*Pruppacher and Jaenicke*, 1995], with significant increases in solubility with each cycle [*Wurzler et al*., 2000]. *R. Kumar et al*. [2011] have argued that even freshly produced dust and mineral aerosols could be significantly hygroscopic; this could be further enhanced by cloud processes [*Crumeyrolle et al*., 2008]. However, these aspects must be explored further.

5. Summary and Conclusions

The present study, which addresses CCN activity from biomass burning and regional background aerosols, is significant because of the highly anthropogenic nature of IGP aerosols. The results are based on measurements from a high-altitude location near the IGP and the limited observations on aerosol-cloud interactions over

southern Asia. Additional quantitative comparisons of particles, based on aerosol chemical compositions, internal and/or external mixing, and physical and optical properties, will be necessary to fully understand the role of aerosols in cloud formation.

The main conclusions of this study are as follows:

1. Both CN and CCN concentrations are higher during the dry autumn and winter seasons when convection is weak and the atmospheric boundary layer is shallow.
2. The AR (fraction of CN that forms CCN) at any given SS varies with the season, peaks in the dry autumn (dominated by biomass smoke), but decreases to a minimum in the wet summer monsoon season. During the study period, the monthly mean CCN AR (at SS = 0.46) was highest (>0.7) in November and lowest (<0.4) in June.
3. The association of CCN activity with the simultaneous optical properties of aerosols shows a strong correlation of CCN with the fine-mode absorption coefficient (σ_{abs}) during autumn. Although the correlations of CCN with scattering aerosols are also high in November, the lower SSA in autumn indicates a relatively higher fraction of absorbing aerosols when the CCN AR is also higher. The relationships between aerosol SSAs and ARs indicate that despite the relatively higher dominance of the absorbing fraction of aerosols (SSA < 0.8), higher CCN concentrations prevail in autumn and winter than in seasons when the scattering fraction of aerosols dominates (SSA > 0.85).

Acknowledgments

This study was conducted as a part of the RAWEX-GVAX experiment by the Indian Space Research Organization, India, and the U.S. Department of Energy (DOE). We acknowledge the U.S. DOE Atmospheric Radiation Measurement (ARM) Climate Research Facility (http://www.arm.gov/sites/amf/pgh/, data: http://www.archive.arm.gov/discovery/#v/results/s/fcat::aeros/fsite::pgh) for providing the database for this work. HYSPLIT transport and dispersion model data (NOAA ARL) were obtained from the READY website (http://www.arl.noaa.gov/ready.html) for back trajectory analysis. The MODIS fire count data used in this study were acquired using the GES-DISC Interactive Online Visualization and analysis Infrastructure as part of the NASA's Goddard Earth Sciences Data and Information Services Center.

References

Acker, K., S. Mertes, D. Moller, W. Wieprecht, R. Auel, and D. Kalasz (2002), Case study of cloud physical and chemical processes in low clouds at Mt. Brocken, *Atmos. Res.*, *64*, 41–51.

Adhikary, B., G. R. Carmichael, Y. Tang, L. R. Leung, Y. Qian, J. J. Schauer, E. A. Stone, V. Ramanathan, and M. V. Ramana (2007), Characterization of the seasonal cycle of south Asian aerosols: A regional-scale modeling analysis, *J. Geophys. Res.*, *112*, D22S22, doi:10.1029/2006JD008143.

Anderson, T. L., and J. A. Ogren (1998), Determining aerosol radiative properties using the TSI 3563 integrating nephelometer, *Aerosol Sci. Tech.*, *29*, 57–69.

Andreae, M. O., and D. Rosenfeld (2008), Aerosol cloud-precipitation interactions. Part 1. The nature and sources of cloud-active aerosols, *Earth Sci. Rev.*, *89*, 13–41.

Babu, S. S., K. K. Moorthy, R. K. Manchanda, P. R. Sinha, S. K. Satheesh, D. P. Vajja, S. Srinivasan, and V. H. Arun Kumar (2011), Free tropospheric black carbon aerosol measurements using high altitude balloon: Do BC layers build "their own homes" up in the atmosphere?, *Geophys. Res. Lett.*, *38*, L08803, doi:10.1029/2011GL046654.

Bauer, S. E., Y. Balkanski, M. Schulz, D. A. Hauglustaine, and F. Dentener (2004), Global modeling of heterogeneous chemistry on mineral aerosol surfaces: Influence on tropospheric ozone chemistry and comparison to observations, *J. Geophys. Res.*, *109*, D02304, doi:10.1029/2003JD003868.

Bergstrom, R. W., P. Pilewskie, P. B. Russell, J. Redemann, T. C. Bond, P. K. Quinn, and B. Sierau (2007), Spectral absorption properties of atmospheric aerosols, *Atmos. Chem. Phys.*, *7*, 5937–5943.

Bollasina, M., S. Nigam, and K. M. Lau (2008), Absorbing aerosols and summer monsoon evolution over South Asia: An observational portrayal, *J. Clim.*, *21*, 3221–3239, doi:10.1175/2007JCLI2094.

Bond, T. C. (2001), Spectral dependence of visible light absorption by carbonaceous particles emitted from coal combustion, *Geophys. Res. Lett.*, *28*(21), 4075–4078, doi:10.1029/2001GL013652.

Burkart, J., G. Steiner, G. Reischl, and R. Hitzenberger (2011), Long-term study of cloud condensation nuclei (CCN) activation of the atmospheric aerosol in Vienna, *Atmos. Environ.*, *45*, 5751–5759.

Crumeyrolle, S., L. Gomes, P. Tulet, A. Matsuki, A. Schwarzenboeck, and K. Crahan (2008), Increase of the aerosol hygroscopicity by cloud processing in a mesoscale convective system: A case study from the AMMA campaign, *Atmos. Chem. Phys.*, *8*, 6907–6924.

Dipu, S., T. V. Prabha, G. Pandithurai, J. Dudhia, G. Pfister, K. Rajesh, and B. N. Goswami (2013), Impact of elevated aerosol layer on the cloud macrophysical properties prior to monsoon onset, *Atmos. Environ.*, *70*, 454–467.

Dumka, U. C., K. K. Moorthy, P. Pant, P. Hegde, R. Sagar, and K. Pandey (2008), Physical and optical characteristics of atmospheric aerosols during ICARB at Manora Peak, Nainital: A sparsely inhabited, high-altitude location in the Himalayas, *J. Earth Syst. Sci.*, *117*(S1), 399–405.

Dumka, U. C., K. K. Moorthy, R. Kumar, P. Hegde, R. Sagar, P. Pant, N. Singh, and S. S. Babu (2010), Characteristics of aerosol black carbon mass concentration over a high-altitude location in the central Himalayas from multiyear measurements, *Atmos. Res.*, *96*, 510–521.

Dusek, U., et al. (2006), Size matters more than chemistry in controlling which particles can nucleate cloud droplets, *Science*, *312*, 1375–1378.

Falkovich, A. H., G. Schkolnik, E. Ganor, and Y. Rudich (2004), Adsorption of organic compounds pertinent to urban environments onto mineral dust particles, *J. Geophys. Res.*, *109*, D02208, doi:10.1029/2003JD003919.

Fitzgerald, J. W. (1973), Dependence of the supersaturation spectrum of CCN on aerosol size distribution and composition, *J. Atmos. Sci.*, *30*, 628–634.

Fletcher, N. H. (1962), *The Physics of Rain Clouds*, Cambridge Univ. Press, Cambridge, U. K.

Furutani, H., M. Dallosto, G. C. Roberts, and K. A. Prather (2008), Assessment of the relative importance of atmospheric aging on CCN activity derived from field observations, *Atmos. Environ.*, *42*, 3130–3142.

Gao, S., D. A. Hegg, P. V. Hobbs, T. W. Kirchstetter, B. I. Magi, and M. Sadilek (2003), Water-soluble organic components in aerosols associated with Savanna fires in Southern Africa: Identification, evolution, and distribution, *J. Geophys. Res.*, *108*(D13), 8491, doi:10.1029/2002JD002324.

Gautam, R., N. C. Hsu, K. M. Lau, and M. Kafatos (2009), Aerosol and rainfall variability over the Indian monsoon region: Distributions, trends and coupling, *Ann. Geophys.*, *27*, 3691–3703.

Gautam, R., et al. (2011), Accumulation of aerosols over the Indo-Gangetic plains and southern slopes of the Himalayas: Distribution, properties and radiative effects during the 2009 premonsoon season, *Atmos. Chem. Phys.*, *11*, 12,841–12,863.
Gibson, E. R., K. M. Gierlus, P. K. Hudson, and V. H. Grassian (2007), Generation of internally mixed insoluble and soluble aerosol particles to investigate the impact of atmospheric aging and heterogeneous processing on the CCN activity of mineral dust aerosol, *Aerosol Sci. Technol.*, *41*(10), 914–924.
Giglio, L., I. Csiszar, and C. O. Justice (2006), Global distribution and seasonality of active fires as observed with the Terra and Aqua Moderate Resolution Imaging Spectroradiometer (MODIS) sensors, *J. Geophys. Res.*, *111*, G02016, doi:10.1029/2005JG000142.
Girolamo, L., T. C. Bond, D. Bramer, D. J. Diner, F. Fettinger, R. A. Kahn, J. V. Martonchik, M. V. Ramana, V. Ramanathan, and P. J. Rasch (2004), Analysis of Multi-angle Imaging Spectroradiometer [MISR] aerosol optical depths over greater India during winter 2001–2004, *Geophys. Res. Lett.*, *31*, L23115, doi:10.1029/2004GL021273.
Gogoi, M. M., S. S. Babu, K. K. Moorthy, M. R. Manoj, and J. C. Chaubey (2013), Absorption characteristics of aerosols over the northwestern region of India: Distinct seasonal signatures of biomass burning aerosols and mineral dust, *Atmos. Environ.*, *73*, 92–102.
Gorbunov, B., and R. Hamilton (1997), Water nucleation on aerosol particles containing both soluble and insoluble substances, *J. Aerosol Sci.*, *28*, 239–248.
Habib, G., C. Venkataraman, I. Chiapello, S. Ramachandran, O. Boucher, and M. S. Reddy (2006), Seasonal and interannual variability in absorbing aerosols over India derived TOMS: Relationship to regional meteorology and emissions, *Atmos. Environ.*, *40*, 1909–1921.
Harrison, L. (1985), The segregation of aerosols by cloud-nucleating activity. Part II: Observation of an urban aerosol, *J. Clim. Appl. Meteorol.*, *24*, 312–321.
Hegde, P., P. Pant, M. Naja, U. C. Dumka, and R. Sagar (2007), South Asian dust episode in June 2006: Aerosol observations in the central Himalayas, *Geophys. Res. Lett.*, *34*, L23802, doi:10.1029/2007GL030692.
Jefferson, A. (2010), Empirical estimates of CCN from aerosol optical properties at four remote sites, *Atmos. Chem. Phys.*, *10*, 6855–6861.
Jefferson, A. (2011), *Aerosol Observing System (AOS) Handbook*, ARM-TR-014, US Department of Energy, Washington, D. C.
Johnson, B. T., S. R. Osborne, J. M. Haywood, and M. A. J. Harrison (2008), Aircraft measurements of biomass burning aerosol over West Africa during DABEX, *J. Geophys. Res.*, *113*, D00C06, doi:10.1029/2007JD009451.
Junge, C. E., and E. McLaren (1971), Relationship of cloud nuclei spectra to aerosol size distribution and composition, *J. Atmos. Sci.*, *28*, 382–390.
Juranyi, Z., M. Gysel, E. Weingartner, P. F. DeCarlo, L. Kammermann, and U. Baltensperger (2010), Measured and modelled cloud condensation nuclei number concentration at the high alpine site Jungfraujoch, *Atmos. Chem. Phys.*, *10*, 7891–7906.
Kirchstetter, T. W., T. Novakov, and P. V. Hobbs (2004), Evidence that the spectral dependence of light absorption by aerosols is affected by organic carbon, *J. Geophys. Res.*, *109*, D21208, doi:10.1029/2004JD004999.
Kotamarthi, V. R., and S. K. Satheesh (2011), *Ganges Valley Aerosol Experiment, em, The Magazine for Environmental Managers*, Air & Waste Management Association, Pittsburgh, Pa.
Kumar, A., M. M. Sarin, and B. Srinivas (2010), Aerosol iron solubility over Bay of Bengal: Role of anthropogenic sources and chemical processing, *Mar. Chem.*, *121*, 167–175, doi:10.1016/j.marchem.2010.04.005.
Kumar, P., I. N. Sokolik, and A. Nenes (2011), Measurements of cloud condensation nuclei activity and droplet activation kinetics of fresh unprocessed regional dust samples and minerals, *Atmos. Chem. Phys.*, *11*, 3527–3541.
Kumar, R., M. Naja, S. K. Satheesh, N. Ojha, H. Joshi, T. Sarangi, P. Pant, U. C. Dumka, P. Hegde, and S. Venkataramani (2011), Influences of the springtime northern Indian biomass burning over the central Himalayas, *J. Geophys. Res.*, *116*, D19302, doi:10.1029/2010JD015509.
Kumar, R., M. C. Barth, G. G. Pfister, M. Naja, and G. P. Brasseur (2014), WRF-Chem simulations of a typical premonsoon dust storm in northern India: Influences on aerosol optical properties and radiation budget, *Atmos. Chem. Phys.*, *14*, 2431–2446.
Lack, D. A., C. D. Cappa, D. S. Covert, T. Baynard, P. Massoli, B. Sierau, T. S. Bates, P. K. Quinn, E. R. Lovejoy, and A. R. Ravishankara (2008), Bias in filter-based aerosol light absorption measurements due to organic aerosol loading: Evidence from ambient measurements, *Aerosol Sci. Technol.*, *42*(12), 1033–1041.
Lammel, G., and T. Novakov (1995), Water nucleation properties of carbon black and diesel soot particles, *Atmos. Environ.*, *29*, 813–823.
Lathem, T. L., A. J. Beyersdorf, K. L. Thornhill, E. L. Winstead, M. J. Cubison, A. Hecobian, J. L. Jimenez, R. J. Weber, B. E. Anderson, and A. Nenes (2013), Analysis of CCN activity of Arctic aerosol and Canadian biomass burning during summer 2008, *Atmos. Chem. Phys.*, *13*, 2735–2756.
Lau, K. M., M. K. Kim, and K. M. Kim (2006), Asian summer monsoon anomalies induced by aerosol direct forcing: The role of the Tibetan Plateau, *Clim. Dyn.*, *26*(7–8), 855–864, doi:10.1007/s00382-006-0114-z.
Lawrence, M. G., and J. Lelieveld (2010), Atmospheric pollutant outflow from southern Asia: A review, *Atmos. Chem. Phys.*, *10*, 11,017–11,096.
Leaitch, W. R., S.-M. Li, P. S. K. Liu, C. M. Banic, A. M. Macdonald, G. A. Isaac, M. D. Couture, and J. W. Strapp (1996), Relationships among CCN, aerosol size distribution and ion chemistry from airborne measurements over the Bay of Fundy in August-September, 1995, in *Nucleation and Atmospheric Aerosols*, edited by M. Kulmala and P. Wagner, pp. 840–843, Elsevier Science Inc.
Lee, S., Y. S. Ghim, S. W. Kim, and S. C. Yoon (2010), Effect of biomass burning and regional background aerosols on CCN activity derived from airborne in situ measurements, *Atmos. Environ.*, *44*, 5227–5236.
Li, W., P. Li, G. Sun, S. Zhou, Q. Yuan, and W. Wang (2011), Cloud residues and interstitial aerosols from nonprecipitating clouds over an industrial and urban area in northern China, *Atmos. Environ.*, *45*, 2488–2495.
Liu, J., and Z. Li (2014), Estimation of cloud condensation nuclei concentration from aerosol optical quantities: Influential factors and uncertainties, *Atmos. Chem. Phys.*, *14*, 471–483.
Manoharan, V. S., R. Kotamarthi, Y. Feng, and M. P. Cadeddu (2014), Increased absorption by coarse aerosol particles over the Gangetic–Himalayan region, *Atmos. Chem. Phys.*, *14*, 1159–1165.
Marinoni, A., et al. (2010), Aerosol mass and black carbon concentrations: A two year record at NCO-P [5079 m, Southern Himalayas], *Atmos. Chem. Phys.*, *10*, 8551–8562.
Massie, S. T., O. Torris, and S. J. Smith (2004), Total Ozone Mapping Spectrometer (TOMS) observations of increases in Asian aerosol in winter from 1979 to 2000, *J. Geophys. Res.*, *109*, D18211, doi:10.1029/2004JD004620.
McFiggans, G., et al. (2006), The effect of physical and chemical aerosol properties on warm cloud droplet activation, *Atmos. Chem. Phys.*, *5*, 8507–8646.
Moorthy, K. K., S. Suresh Babu, S. K. Satheesh, J. Srinivasan, and C. B. S. Dutt (2007), Dust absorption over the "Great Indian Desert" inferred using ground-based and satellite remote sensing, *J. Geophys. Res.*, *112*, D09206, doi:10.1029/2006JD007690.
Moorthy, K. K., S. S. Babu, M. R. Manoj, and S. K. Satheesh (2013), Buildup of Aerosols over the Indian Region, *Geophys. Res. Lett.*, *40*, 1011–1014, doi:10.1002/GRL.50165.
Nair, V. S., et al. (2007), Wintertime aerosol characteristics over the Indo-Gangetic Plain [IGP]: Impacts of local boundary layer processes and long-range transport, *J. Geophys. Res.*, *112*, D13205, doi:10.1029/2006JD008099.

Pandithurai, G., S. Dipu, T. V. Prabha, R. S. Maheskumar, J. R. Kulkarni, and B. N. Goswami (2012), Aerosol effect on droplet spectral dispersion in warm continental cumuli, *J. Geophys. Res.*, *117*, D16202, doi:10.1029/2011JD016532.

Petzold, A., M. Gysel, X. Vancassel, R. Hitzenberger, H. P. Uxbaum, S. Vrochticky, E. Weingartner, U. Baltensperger, and P. Mirabel (2005), On the effects of organic matter and sulphur-containing compounds on the CCN activation of combustion particles, *Atmos. Chem. Phys.*, *5*, 3187–3203.

Pierce, J. R., and P. J. Adams (2009), Uncertainty in global CCN concentrations from uncertain aerosol nucleation and primary emission rates, *Atmos. Chem. Phys.*, *9*, 1339–1356.

Prasad, A. K., R. P. Singh, and A. Singh (2004), Variability of aerosol optical depth over Indian Subcontinent: Trend and departures in recent years, *J. Indian Soc. Remote Sens.*, *32*(4), 313–316.

Pruppacher, H. R., and R. Jaenicke (1995), The processing of water vapor and aerosols by atmospheric clouds: A global estimate, *Atmos. Res.*, *38*, 283–295.

Pruppacher, H. R., and J. D. Klett (1978), *Microphysics of Clouds and Precipitations*, D. Reidel Co., Dordrecht, Netherlands.

Ram, K., M. M. Sarin, and P. Hegde (2008), Atmospheric abundances of primary and secondary carbonaceous species at two high-altitude sites in India: Sources and temporal variability, *Atmos. Environ.*, *42*, 6785–6796.

Ram, K., M. M. Sarin, and P. Hegde (2010), Long-term record of aerosol optical properties and chemical composition from a high-altitude site (Manora Peak) in Central Himalaya, *Atmos. Chem. Phys.*, *10*, 11,791–11,803.

Ramanathan, V., et al. (2001), Indian Ocean Experiment: An integrated analysis of the climate forcing and effects of the great Indo-Asian haze, *J. Geophys. Res.*, *106*(D22), 28,371–28,398, doi:10.1029/2001JD900133.

Ramanathan, V., C. Chung, D. Kim, T. Bettge, L. Buja, J. T. Kiehl, W. M. Washington, Q. Fu, D. R. Sikka, and M. Wild (2005), Atmospheric brown clouds: Impacts on South Asian climate and hydrological cycle, *Proc. Natl. Acad. Sci. U.S.A.*, *102*, 5326–5333.

Ramanathan, V., M. V. Ramana, G. Roberts, D. Kim, C. Corrigan, C. Chung, and D. Winker (2007), Warming trends in Asia amplified by brown cloud solar absorption, *Nature*, *448*, 575–578.

Rose, D., A. Nowak, P. Achtert, A. Wiedensohler, M. Hu, M. Shao, Y. Zhang, M. O. Andreae, and U. Pöschl (2010), Cloud condensation nuclei in polluted air and biomass burning smoke near the mega-city Guangzhou, China, part-1: Size resolved measurements and implications for the modeling of aerosol particle hygroscopicity and CCN activity, *Atmos. Chem. Phys.*, *10*, 3365–3383.

Russell, L. M., S. F. Maria, and S. C. B. Myneni (2002), Mapping organic coatings on atmospheric particles, *Geophys. Res. Lett.*, *29*(16), 26-1–26-4, doi:10.1029/2002GL014874.

Sagar, R., B. Kumar, U. C. Dumka, K. K. Moorthy, and P. Pant (2004), Characteristics of aerosol spectral optical depths over Manora Peak: A high-altitude station in the central Himalayas, *J. Geophys. Res.*, *109*, D06207, doi:10.1029/2003JD003954.

Sarkar, S., R. Chokngamwong, G. Cervone, R. P. Singh, and M. Kafatos (2006), Variability of aerosol optical depth and aerosol forcing over India, *Adv. Space Res.*, *37*(12), 2153–2159.

Satheesh, S. K., K. K. Moorthy, S. S. Babu, V. Vinoj, and C. B. S. Dutt (2008), Climate implications of large warming by elevated aerosol over India, *Geophys. Res. Lett.*, *35*, L19809, doi:10.1029/2008GL034944.

Saxena, P., L. M. Hildemann, P. H. McMurry, and J. H. Seinfeld (1995), Organics alter hygroscopic behavior of atmospheric particles, *J. Geophys. Res.*, *100*, 18,755–18,770, doi:10.1029/95JD01835.

Schwarz, J. P., et al. (2008), Measurement of the mixing state, mass, and optical size of individual black carbon particles in urban and biomass burning emissions, *Geophys. Res. Lett.*, *35*, L13810, doi:10.1029/2008GL033968.

Seinfeld, J. H., and S. N. Pandis (1998), *Atmospheric Chemistry and Physics: From Air Pollution to Climate Change*, 710 pp., Wiley, New York.

Semeniuk, T. A., M. E. Wise, S. T. Martin, L. M. Russell, and P. R. Buseck (2007), Hygroscopic behavior of aerosol particles from biomass fires using environmental transmission electronic microscopy, *J. Atmos. Chem.*, *56*, 259–273.

Sihto, S. L., et al. (2011), Seasonal variation of CCN concentrations and aerosol activation properties in boreal forest, *Atmos. Chem. Phys.*, *11*, 13,269–13,285.

Srivastava, A. K., S. Tiwari, P. C. S. Devara, D. S. Bisht, M. K. Srivastava, S. N. Tripathi, P. Goloub, and B. N. Holben (2011), Pre-monsoon aerosol characteristics over the Indo-Gangetic Basin: Implications to climatic impact, *Ann. Geophys.*, *29*, 789–804.

Srivastava, A. K., S. N. Tripathi, S. Dey, V. P. Kanawade, and S. Tiwari (2012), Inferring aerosol types over the Indo-Gangetic Basin from ground-based sunphotometer measurements, *Atmos. Res.*, *109–110*, 64–75.

Stevens, B., and G. Feingold (2009), Untangling aerosols effects on clouds and precipitation in a buffered system, *Nature*, *461*, 607–613, doi:10.1038/nature08281.

Sun, J., and P. A. Ariya (2006), Atmospheric organic and bio-aerosols as cloud condensation nuclei (CCN): A review, *Atmos. Environ.*, *40*, 795–820.

Twohy, C. H., and J. R. Anderson (2008), Droplet nuclei in nonprecipitating clouds: Composition and size matter, *Environ. Res. Lett.*, *3*, doi:10.1088/1748-9326/3/4/045002.

Twohy, C. H., et al. (2009), Saharan dust particles nucleate droplets in eastern Atlantic clouds, *Geophys. Res. Lett.*, *36*, L01807, doi:10.1029/2008GL035846.

Venkataraman, C., G. Habib, D. Kadamba, M. Shrivastava, J.-F. Leon, B. Crouzille, O. Boucher, and D. G. Streets (2006), Emissions from open biomass burning in India: Integrating the inventory approach with high-resolution Moderate Resolution Imaging Spectroradiometer (MODIS) active-fire and land cover data, *Global Biogeochem. Cycles*, *20*, GB2013, doi:10.1029/2005GB002547.

Vinoj, V., and S. K. Satheesh (2004), Direct and indirect radiative effects of sea salt aerosols over Arabian Sea, *Curr. Sci.*, *86*(10), 1381–1390.

Virkkula, A. (2010), Correction of the calibration of the 3-wavelength particle soot absorption photometer (3λ PSAP), *Aerosol Sci. Technol.*, *44*(8), 706–712.

Wurzler, S., T. G. Reisin, and Z. Levin (2000), Modification of mineral dust particles by cloud processing and subsequent effects on drop size distributions, *J. Geophys. Res.*, *105*, 4501–4512, doi:10.1029/1999JD900980.

Zhang, R., A. F. Khalizov, J. Pagels, D. Zhang, H. Xue, and P. H. McMurry (2008), Variability in morphology, hygroscopicity, and optical properties of soot aerosols during atmospheric processing, *Proc. Natl. Acad. Sci. U.S.A.*, *105*, 10,291–10,296.